

Targeted Nanomedicine: Ashvattha Therapeutics' Path to Developing Hydroxyl Dendrimers

Table of Contents

I. Executive Summary.....	3
II. Introduction	3
III. Hydroxyl Dendrimers (HDs)	3
1) HD charge and surface influence uptake in activated cells.....	4
2) HD size and surface properties influence clearance	5
IV. Drug Conjugation to HDs	5
V. Preclinical studies	7
A. Ophthalmology.....	7
B. Neurology	9
C. Systemic disease.....	11
1) Systemic inflammation.....	11
2) Arthritis.....	12
3) Acute renal injury	12
4) Acute myocardial infarction	13
5) Acute lung injury	13
6) Neuromuscular disease	13
VI. HDs in the Clinic.....	13
i) D-4517.2 (migladendranib)	13
ii) OP-801 (“flurimedrimer”).....	14
iii) OP-101 (“acetylcysteine zidrimer”)	14
VII. Conclusion	16
VIII. Tables.....	17
Table 1. Dendrimer Characteristics	17
Table 2. Ocular Localization.....	17
Table 3. Ocular Efficacy.....	18
Table 4. CNS Localization.....	19
Table 5. Efficacy in Animal Models of CNS Diseases.....	20
Table 6. Localization in Other Systemic Disease Models.....	22
Table 7. Clinical Trial Efficacy.....	22
IX. Literature Cited	23

I. Executive Summary

Ashvattha Therapeutics (Ashvattha) is advancing novel, clinical-stage precision nanomedicine therapeutics in ophthalmology, neurology and inflammatory disease based on hydroxyl dendrimers (HD), its proprietary nanomedicine technology. Ashvattha's nanomedicines can be administered systemically to treat patients with neuroinflammatory and ocular diseases because their unique surface properties allow them to traverse the blood-brain barrier (BBB) and blood-retinal barrier (BRB) in regions of inflammation. Ashvattha's nanomedicine surface properties enable their selective internalization by activated cells in regions of inflammation while bypassing healthy cells. This unique approach of selectively targeting cells within regions of inflammation provides a safe therapeutic option to address difficult-to-treat diseases and offers a treatment tailored to the inflammation of each patient.

II. Introduction

Dendrimers are nanoparticles that consist of globular molecules composed of branched layers (generations) of repeating units that are radially attached to the interior core.^{1,2} More than 100 dendritic structures have been reported, such as polyamidoamine (PAMAM) dendrimers, polypropyleneimine (PPI) dendrimers, as well as polyamide-, polyether-, polyester-, and phosphorus-based dendrimers. Factors determining dendrimer properties are chemical composition, architecture, size, and surface properties.³

PAMAM dendrimers were among the first produced at scale (up to 1 kg). PAMAM dendrimers are hyperbranched polymers with unparalleled molecular uniformity, defined size and a multifunctional terminal surface. PAMAM are "grown" off a central core in an iterative manufacturing process. The core of PAMAM dendrimers is composed of ethylene diamine; reactions between ethylene diamine molecules grow the dendrimer by doubling the number of functional end groups. Each doubling is known as a "generation". Increasing generations (molecular weight) produce larger molecular diameters, twice the number of reactive surface sites, and approximately double the molecular weight of the preceding generation. The serial reactions and processing between reactions require extended manufacturing times. The original process for manufacturing PAMAM dendrimers was developed by Dendritech, Inc, who scaled the manufacture up to 1 kg while selling dendrimers to researchers and for use in dye processes. Our founders at Johns Hopkins purchased PAMAM dendrimers from Dendritech to evaluate the impact of coating the surface of PAMAM with hydroxyl groups on their ability to target activated cells in regions of inflammation. Because Dendritech could produce the HDs at scale for GLP toxicology and clinical trials, Dendritech was the source for the development of HD therapeutics (HDTs) by Ashvattha.

III. Hydroxyl Dendrimers (HDs)

The size and surface chemistry of the PAMAM dendrimers determine their toxicity and biodistribution.³ Toxicity has been observed when the surface charge is highly positive, generating holes in the cellular lipid bilayer.^{3,4} Modification of the surface by adding hydroxyl groups to create HDs provides an overall neutral charge with low to absent toxicity.³⁻⁵

A series of experiments examining different functional groups at the surface of PAMAM found certain unique properties when hydroxyl groups were used in this dendrimer architecture. The high density of

surface hydroxyls provides a neutral charge that can escape the vasculature and cross the BBB and BRB with selective uptake by activated macrophages/microglia. Selective uptake by activated macrophages/microglia appears to be mainly driven by fluid-phase endocytosis and is independent of a receptor-mediated process.^{6–10}

Through chemical conjugation of small molecule drugs to the hydroxyl groups on the HD surface, Ashvattha designs novel nanomedicines that target intracellular pathways specifically in activated cells (see **Figure 1**).

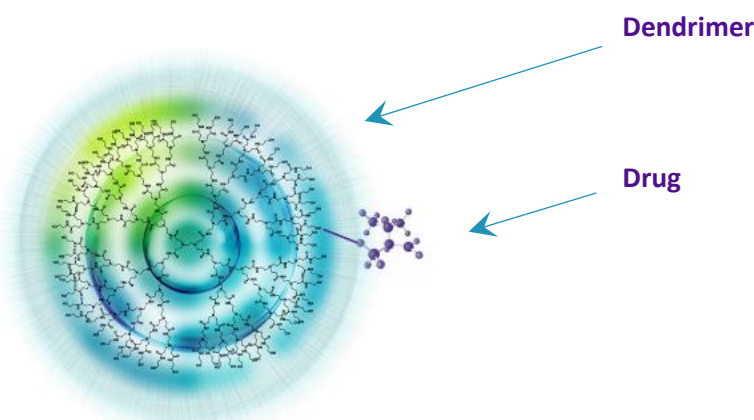


Figure 1. HD. Drug or radioisotope is conjugated to the dendrimer via linker arm.

1) HD charge and surface influence uptake in activated cells

Addition of hydroxyl groups to the dendrimer surface plays a key role in targeting activated cells. This specific targeting is theorized to arise from the high density of surface hydroxyl groups possible with dendrimers due to their unique branching structure (~ 1 OH terminal group/nm² for HD) that is difficult to achieve with other polymeric nanoparticles. The addition of hydroxyl groups to other dendritic structures of similar size and shape such as polyethylene glycol-based dendrimer (PEGOL-60 with ~ 5 OH terminal group/nm²) showed similar targeting properties as HDs with uptake by activated macrophages and microglia.⁵

Resting and activated cells primarily employ fluid phase endocytosis to internalize HDs in cell culture experiments.¹¹ Cellular endocytosis is stimulated in the presence of inflammatory stimuli such as lipopolysaccharide (LPS), resulting in greater internalization of neutral HDs without influencing their retention time in the cell.¹¹ In contrast to neutral HDs, LPS stimulation only modestly increases anionic HD uptake, highlighting the importance of the neutral charge for HD uptake by activated cells.¹² HD uptake is significantly inhibited when pinocytosis, aquaporin and mannose pathways are blocked, suggesting that HDs may employ multiple mechanisms such as fluid phase micropinocytosis, caveolae-mediated endocytosis and phagocytosis.¹¹

The preferential accumulation of HDs in activated microglia/macrophages within regions of inflammation was confirmed in studies using brain slices and in animal models of neurological diseases.^{9,13–15} Upon brain injury, microglia undergo a pronounced change in morphology from a ramified to an amoeboid structure associated with a concomitant decrease in their migratory ability.

Amoeboid microglia internalize HDs more rapidly and to a greater extent than ramified “resting” microglia.^{9,15,16} In Alzheimer’s disease, the greatest inflammatory reaction was observed around amyloid beta (A β) plaques, which are surrounded by microglia with an amoeboid “activated” morphology in humans^{17–19} and mouse models of the disease.^{13,20} In the 5xFAD mouse model, neutral HDs preferentially accumulated in A β plaque-associated microglia, which are considered “hyperactivated” due to their abnormal amoeboid morphology.¹³ In this model, astrocytes, oligodendrocytes and neurons did not internalize HDs, again reinforcing the specific targeting of activated cells.¹³

2) HD size and surface properties influence clearance

Plasma-binding properties and particle size are two major factors that drive drug clearance. Particles with a hydrophobic or charged surface are more likely to interact with and bind to circulating plasma proteins. Due to their neutral surface charge, HDs have weak interactions with human plasma proteins.²¹ Therefore, HD size is the main factor driving their clearance mechanism. Particles with a diameter below 6-8 nm are efficiently cleared by glomerular filtration.²² G4 (64 surface hydroxyls) and G6 (256 surface hydroxyls) HDs have diameters ~4.2 nm and 6.7 nm, respectively, and similar surface properties (neutral and hydrophilic). However, G6 HD size (~1.5-fold larger than G4) lies on the edge of the renal filtration range, which can affect circulation half-life and renal clearance. Biodistribution studies using different animal species (rodents and canine) showed that renal elimination is the predominant clearance mechanism of G4 HDs.^{9,23–27} In contrast, G6 HDs have reduced renal clearance and enhanced liver (sinusoids) and spleen (red pulp) accumulation compared to G4 HDs, indicating involvement of the reticuloendothelial system (RES) system in G6 HD clearance^{24,26} (see **Table 1**). Ashvattha currently only uses G4 PAMAM HDs for its products targeting the CNS and eye.

In conclusion, Ashvattha selected Generation 4 (G4) PAMAM with 64 surface hydroxyl groups as an optimal core technology for neurology and ophthalmology indications because: 1) size and globular shape allow renal clearance via glomerular filtration while Generation 6 (G6) and higher generations rely more on hepatic clearance; 2) surfaces can be chemically tailored²⁸ to target activated cells by adding hydroxyl groups to the HD providing an overall neutral charge and low to absent toxicity; and 3) they have been safely administered to healthy volunteers and patients with COVID-19.

IV. Drug Conjugation to HDs

In the original work from Johns Hopkins, drug compounds were linked through various spacer arms connected to the HD surface primarily by ester bonds. These early HDTs were prodrugs intended to release the conjugated drug inside activated cells. The only clinical stage HDT that is a prodrug is OP-101 (acetylcysteine zidrimmer) (see **Table 1**). Ashvattha is not currently using this first-generation approach to develop new drug candidates.

To avoid the potential release of active drug in the systemic circulation, Ashvattha optimized conjugation chemistry. For two clinical-stage compounds (D-4517.2 and OP-801), HDs are produced with a set number of ether linker PEG-alkyne arms in place of hydroxyls on the surface (see **Table 1**). These alkyne arms are then reacted with azide-terminated drugs or radioisotope carriers using click chemistry. This approach results in metabolically stable HDTs with an ether linkage to the HD and no hydrolysable bonds. Ashvattha produced metabolically stable HDTs with biochemical and biological potency comparable to small molecule analogs. In particular, D-4517.2 was designed to have 7 to 8 vascular

endothelial growth factor receptor (VEGFR) tyrosine kinase inhibitors with nanomolar binding affinity and potent *in vitro* and *in vivo* inhibition of angiogenesis attached to its surface. D-4517.2 (migladendranib) is the first in a new class of tyrosine kinase inhibitors named dendranibs by the International Nonproprietary Name (INN).

To our knowledge, Ashvattha's [precision medicine technology](#) is the only one that has been shown to selectively target activated cells (microglia/macrophages and activated RPE cells) through a biophysical mechanism independent from receptor binding. This is achieved using a hydroxyl surface density key for diffusion across the BBB and BRB and intracellular uptake in activated cells without the use of targeting ligands (see **Figure 2**).

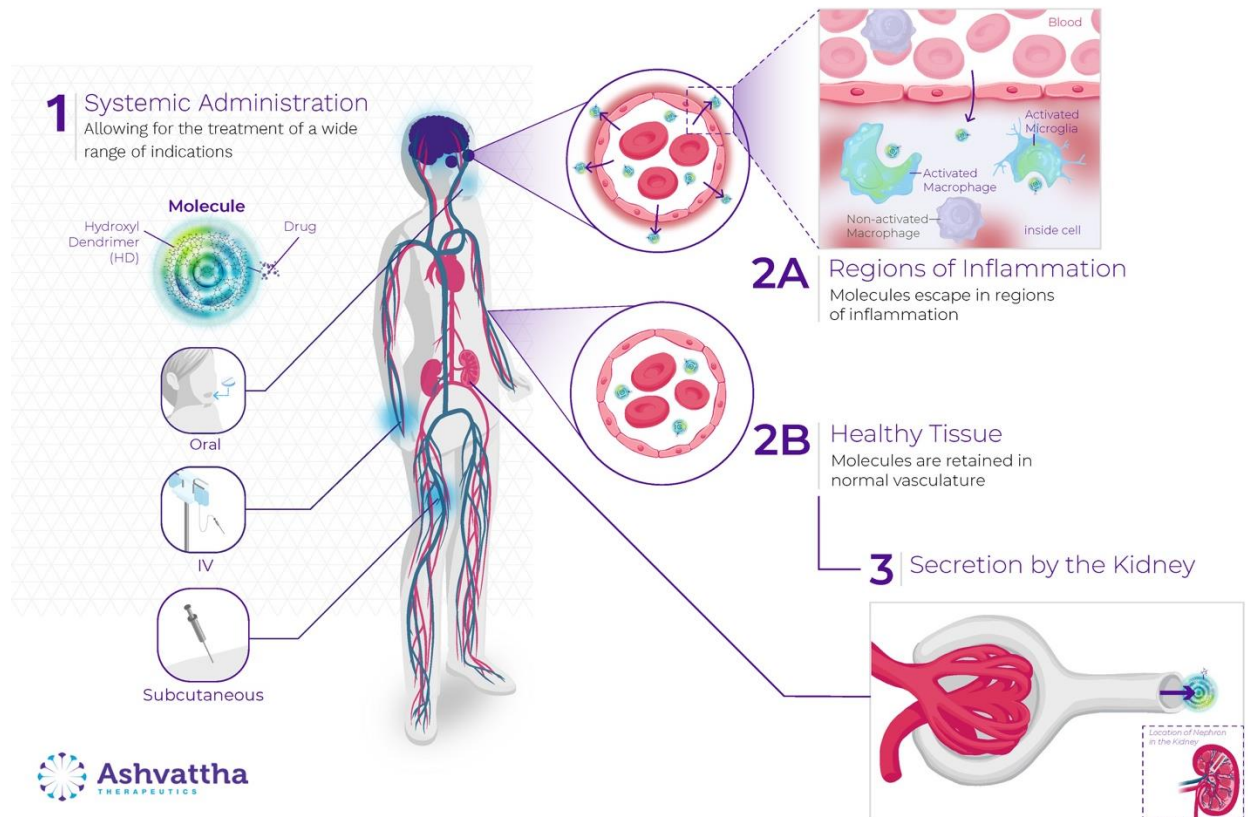


Figure 2: Ashvattha's nanomedicines offer a differentiated mechanism of action (MOA) due to specific targeting of activated cells in areas of injury. Following systemic (intravenous (IV), subcutaneous (SC), or oral) administration, HDs distribute throughout the vasculature (**Figure 2**, step 1). In the presence of inflammation, HDs cross the BBB and BRB to enter inflamed tissue before being internalized via endocytosis by activated macrophages, microglia and retinal pigment epithelial (RPE) cells (**Figure 2**, step 2a). In healthy tissues, they remain in the vasculature and pass through the body (**Figure 2**, step 2b) due to their small size and water-like surface properties. HD therapeutics that are not taken up by cells bypass liver metabolism and are excreted unchanged in the urine within 24-48 hours of administration (**Figure 2**, step 3).

V. Preclinical studies

A. Ophthalmology

1) HDs cross the BRB and are internalized by activated microglia/macrophages and RPE cells specifically in regions of inflammation (**Table 2**)

Ocular distribution was examined after intravitreal (IVT) and systemic administration of HDs to rodent and non-human primate models of retinal degeneration as well as human donor eyecups *in vitro* (see **Table 2**). In rodent models of macular degeneration and retinopathy, G4 HDs accumulated specifically in activated choroidal macrophages as well as activated microglia/macrophages and RPE cells of the retina (see **Figure 3**).⁶⁻⁸

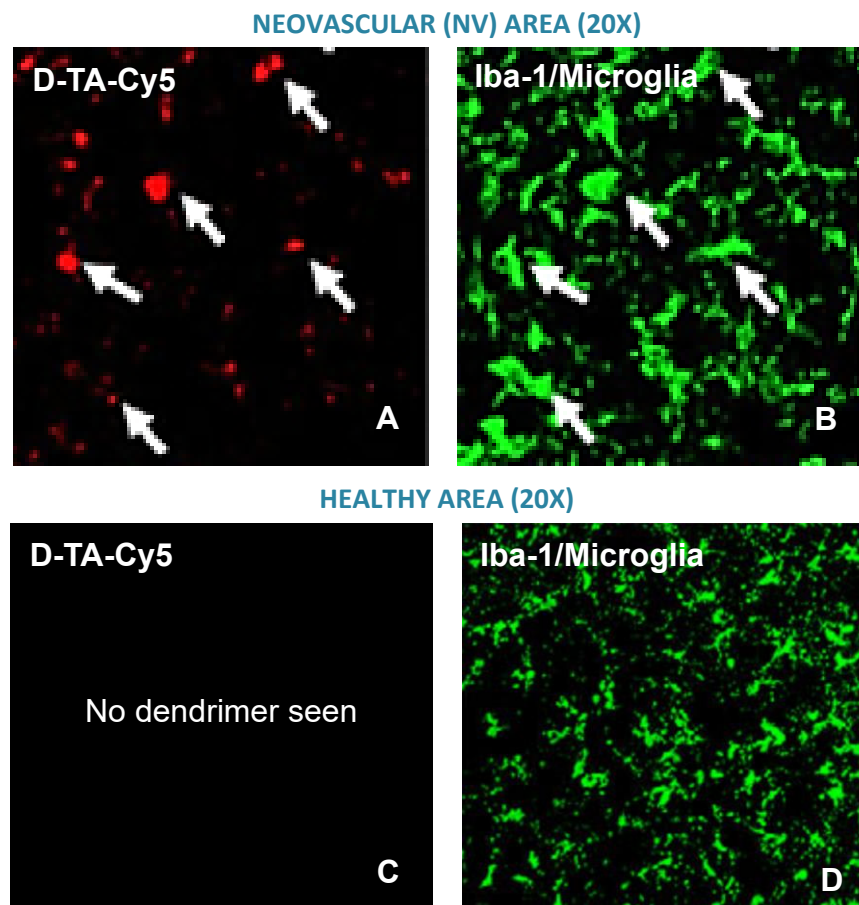


Figure 3. Biodistribution and colocalization of IVT labeled D-TA in retinal tissue of neonatal oxygen-induced retinopathic (OIR) mice. The macrophages/microglia were stained for Iba-1 (green) and D-TA-Cy5 is depicted in red. Flat mount of OIR retina showing activated “amoeboid” microglia containing D-TA-Cy5 within the neovascular area (A, B) and healthy retina containing ramified microglia (non-activated) and normal vasculature without D-TA-Cy5 (C, D). Adapted from Cho *et al.*, 2020.⁸

In these studies, ~65-90% of the microglia/macrophage population in areas of retina/choroid injury accumulated HDs, whereas microglia/macrophages in healthy parts of the eye did not internalize HDs.

This demonstrates efficient and specific cell targeting. Importantly, G4 HDs were retained in microglia up to 13-35 days following injury even after microglia reverted to a resting, ramified morphology.^{6,8,29,30} IV administered G4 HDs at doses 30-300x higher than IVT administration led to similar or superior uptake and retention by activated cells of the retina/choroid in rodent and non-human primate models of ocular neuropathy (**Fig. 4**).^{7,31}

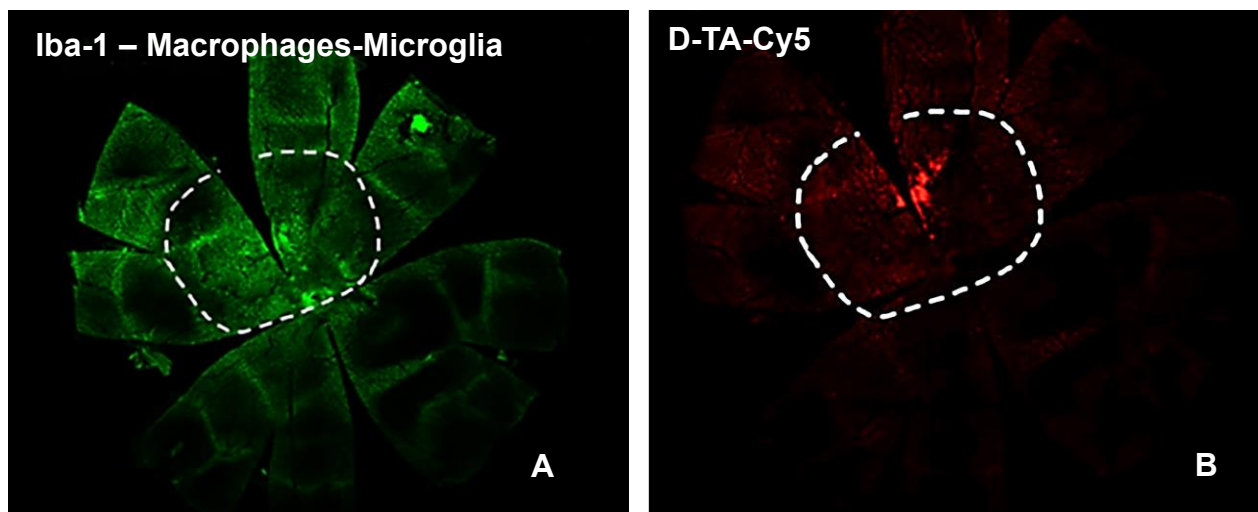


Figure 4. Biodistribution of dendrimer and D-TA-Cy5 in choroidal flat mounts of a rat model for AMD.

The macrophages and microglia were stained for Iba-1 (green) and D-TA-Cy5 is depicted in red. Choroidal flat mount (5x magnification) shows macrophages (A) and accumulation of D-TA-Cy5 (B) specifically in the bleb area (white dotted lines) 7d post IV-administration of D-TA-Cy5 indicating a specific localization of HD within the injured area. Adapted from Kambhampati *et al.*, 2021.⁷

In summary, HDs were internalized by activated microglia/macrophages and RPE cells in injured areas of the retina/choroid, whereas no accumulation was detected in cells from healthy eye tissue. These findings were likely due either to the inability of HDs to traverse the intact BRB or to a lack of uptake by healthy, non-activated cells.

2) G4 HDs accumulate in activated cells in areas of inflammation

In a mouse model of ocular ischemia/reperfusion injury, the amount of G4 HDs localized in activated microglia/macrophages and RPE cells was quantified 24 hours and 21 days after IV administration. The percent of injected dose (%ID) per gram of ocular tissue was ~35% and ~20% 24 hours and 21 days after dosing, respectively.⁶ Immunostaining confirmed that G4 HD accumulation did not occur in surrounding healthy cells of non-injured tissues.

3) HDs have superior efficacy and safety compared to standard of care treatments in ocular diseases (Table 3)

IVT triamcinolone-acetonide (TA) is a corticosteroid drug often used off-label for indications such as diabetic retinopathy (DR), diabetic macular edema (DME) and other ocular inflammatory conditions. While effective, intraocular injection of TA is not the first-choice treatment due to side effects such as elevation of intraocular pressure (IOP), localized retinal toxicity due to formation of epiretinal crystals in the vitreous humor and cataract formation.

Systemic administration of G4 HD conjugated to TA (D-TA) was ~4-fold more effective in preventing choroidal neovascularization (CNV) progression than a 10-fold higher dose of free TA in a rat model of AMD.⁷ Systemic D-TA also had less side effects with minimal IOP increases and no signs of tissue toxicity. Superiority of D-TA in reducing retinal neovascularization and improving visual function compared to free TA was confirmed in a mouse model of ischemic retinopathy.⁸ Similar observations were made with G4 HD conjugated to fluocinolone acetonide (D-FA) to treat retinal inflammation, where D-FA preserved photoreceptor health and outer nuclear layer thickness and attenuated neuroinflammation significantly better than free FA over one month.²⁹

Current front-line treatments for AMD include anti-VEGF agents, which are injected directly into the eye (IVT) and target neovascularization but do not address inflammation or decrease VEGF production.³² These therapies also have a short half-life and can have undesirable side effects. In a laser-induced mouse model, a single SC or oral dose of D-4517.2 (migladendranib), a potent anti-angiogenic HD nanomedicine (see **Table 1**), significantly reduced choroidal neovascularization to levels comparable to IVT aflibercept, the current standard of care for wet AMD and DME.^{33,34}

B. Neurology

1) HDs cross the BBB and are internalized by activated microglia cells specifically in regions of inflammation (Table 4)

HD biodistribution in the brain was examined after IV dosing of G4 and G6 HDs to rodent and canine models of neurological diseases (see **Table 4**). Both G4 and G6 HDs selectively localized in activated microglia in inflamed brain regions and were not detected outside the vasculature in healthy tissues.^{9,10,16,26,35-37} In regions of inflammation, ~60-90% of activated microglia accumulated HDs (see **Figure 5**).^{9,15} Two studies in neonatal mouse and rabbit models reported that a small number (~2-10%) of astrocytes and neurons also internalized HDs^{10,15,24}; however, internalization of HDs in astrocytes was not observed in other animal models and was seen only in necrotic/apoptotic neurons with deformed cell bodies.^{16,24,38} The preferential uptake of HDs by microglia associated with A β plaques and the absence or low uptake of HDs in non-plaque-associated microglia, astrocytes, oligodendrocytes and neurons in 5xFAD mice confirmed selective targeting of HDs to activated microglia.^{39,40} Targeting plaque-associated microglia with HDs without affecting neighboring cells is an attractive therapeutic approach to reduce neuroinflammation associated with A β and tau accumulation in Alzheimer's disease. Importantly, the number of microglia internalizing G4 HDs was positively correlated with their activation status as measured by morphological changes, reinforcing specific targeting of HDs to activated cells.¹⁵ Supporting the specific targeting of HDs to activated microglia in regions of inflammation, the amount of G4 and G6 HD uptake in the brain was correlated with disease severity in a rabbit model of cerebral palsy (CP) and mouse model of sepsis.⁹

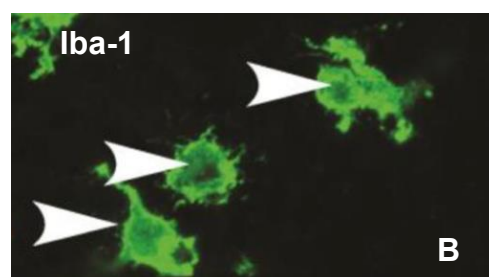
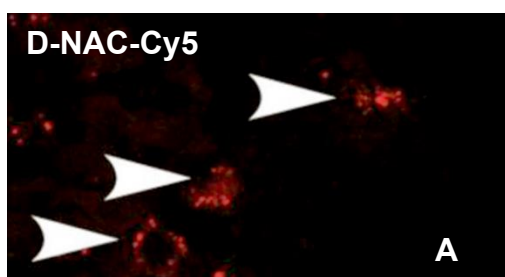


Figure 5. Uptake of D-NAC-Cy5 in microglia. Uptake of D-NAC-Cy5 (red, A) is observed in Iba1+ microglia (green, B) in the hippocampus of CD1 mice undergoing brain hypoxia using a unilateral carotid ligation model. Adapted from Nemeth *et al.*, 2017.¹⁵

The specific targeting of G4 HDs to activated microglia in regions of inflammation was also shown by measuring target engagement. The CX3CR1+ microglia population of mice dosed with G4 HDs conjugated with a glutaminase inhibitor N-(5-{2-[2-(5-amino-[1,3,4]thiadiazol-2-yl)-ethylsulfanyl]-ethyl}-[1,3,4]thiadiazol-2-yl)-2-phenyl-acetamide (D-JHU29) had a reduced glutaminase (GLS) activity that was not observed in the non-microglial (CX3CR1-) cell fraction.⁴¹ Similarly, G4 HDs conjugated with a neutral sphingomyelinase 2 (nSMase2) inhibitor 2,6-Dimethoxy-4-(5-Phenyl-4-Thiophen-2-yl-1H-Imidazol-2-yl)-Phenol (DPTIP) reduced nSMase2 activity in the hippocampus, but not in the frontal cortex, due to the lack of microglial activation in the cortex away from the site of injury induced via AAV hTau injection.⁴² These studies further demonstrate targeting specificity of HD nanomedicines.

2) G4 and G6 HDs accumulate in activated cells in areas of inflammation

Uptake studies estimated that ~0.1-0.2% of the G4 and G6 HDs administered dose was successfully delivered to activated microglia in a rabbit model of CP and in a canine model of brain injury.^{9,24,38} The CSF to blood ratio is an important marker to quantify drug levels crossing the BBB following systemic administration. Importantly, the CSF to serum ratio for G4 HDs was ~1-2%, which is higher than the reported average of ~0.1%-0.3% for antibodies and small molecules.^{24,38} Greater brain accumulation of G4 HDs was observed in the 5xFAD mouse model for Alzheimer's disease, possibly due to differences in BBB impairment across animal models prohibiting G6 dendrimer crossing.^{9,13,24,26,43}

3) Acetylcysteine zidimer (OP-101) and new dendranibs are efficacious in preclinical models of neurological diseases (Table 5)

OP-101 conjugated to N-acetyl cysteine (NAC), reduced microglia-mediated inflammation, demyelination and cognitive impairment after IV or oral administration in several rodent models of neurological disease.^{10,16,43-45} In a rabbit model of CP, a single IV dose of OP-101 reduced neuronal injury and improved motor function in newborn kits, whereas free NAC was not efficacious even at doses 10 times higher than OP-101.¹⁰ This dramatic improvement in motor function was also observed when treating CP newborn kits with G6 HD conjugated with NAC, whereas CP kits treated with free NAC did not survive until the end of the study.⁴³ Superior efficacy of OP-101 over free NAC was reproduced in a mouse model of Rett syndrome in which OP-101 improved neurobehavioral functions.¹⁶ The difference in efficacy between free NAC and OP-101 may stem from poor bioavailability of free NAC and greater accumulation of OP-101 specifically in activated microglia.⁹ Similarly, when equimolar doses of nSMase2 inhibitor (DPTIP) and G4 HD conjugated with DPTIP (D-DPTIP) were administered to block propagation of toxic hyperphosphorylated tau species in mice, oral D-DPTIP was significantly more effective than free DPTIP due to its poor oral bioavailability, modest brain penetration and rapid clearance.⁴⁶ When a glutamate carboxypeptidase II inhibitor (2-PMPA) with poor bioavailability and limited brain penetration was conjugated to G4 HD (D-2PMPA), 17.5-fold lower doses of D-2PMPA compared to the dose of free 2-PMPA were required to significantly improve cognitive functions (see **Figure 6**).³⁶

The superior efficacy of G4 HDs conjugated to small molecule drugs compared to unconjugated free drug was also observed by Ashvattha's collaborators in experimental autoimmune encephalomyelitis (EAE) and 5xFAD mouse models for multiple sclerosis (MS) and Alzheimer's disease, respectively.⁴⁰ In these studies, a new dendranib nanomedicine that selectively inhibits colony-stimulating factor 1 (CSF-1) signaling in microglia (ASH-41020) reduced paralysis in EAE mice and improved anxiety-related behavior in 5xFAD mice.^{40,47}

In addition to superior efficacy, improved safety was observed when conjugating valproic acid (VPA) with G4 HDs. Large VPA doses provide neuroprotection but increase the risk of adverse side effects such as peri-operative hypotension and pulmonary edema/hemorrhage. G4 HD conjugated to VPA required only 1/10th of the free VPA dose to provide similar levels of neuroprotection and reduced systemic toxicity.

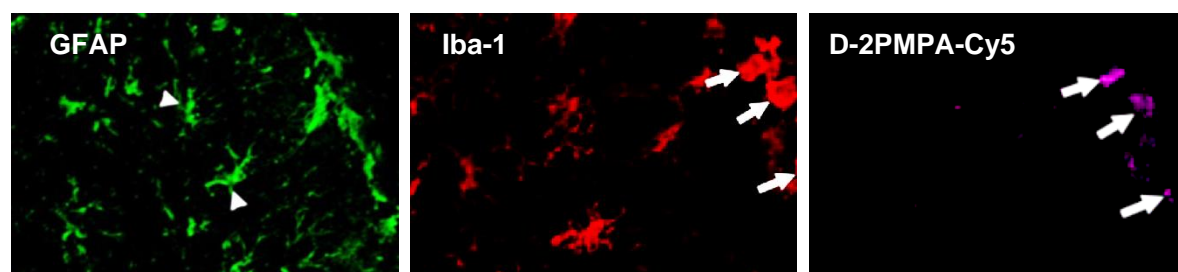


Figure 6. Activated microglia selectively take up D-2PMPA-Cy5 in a mouse model of MS. EAE immunized mice demonstrated no D-2PMPA-Cy5 signal in GFAP positive astrocytes (green). Brain images show selective uptake of D-2PMPA-Cy5 (violet) by Iba1-positive (red) activated microglia along the DG edge (arrows) but not by non-activated (ramified) microglia. Adapted from Hollinger *et al.*, 2022.⁴⁸

C. Systemic disease

Delivery of HDs has been studied in several animal models of systemic inflammatory disease (see **Table 6**). Cumulatively, these data suggest that labeling of activated macrophages occurs in areas of inflammation located in multiple tissues.

- 1) **Systemic inflammation:** To study HD localization in the context of systemic hyperinflammation, ~150 μ Ci of OP-801, an ¹⁸F-conjugated HD designed to be used as a positron emission tomography (PET) imaging agent, was administered to mice following intraperitoneal (IP) injection of 10 mg/kg LPS. Whole body dynamic PET scanning for 60 minutes in live mice showed sensitive and specific visualization of activated macrophage-mediated inflammation throughout the entire body (see **Figure 7**).⁴⁹

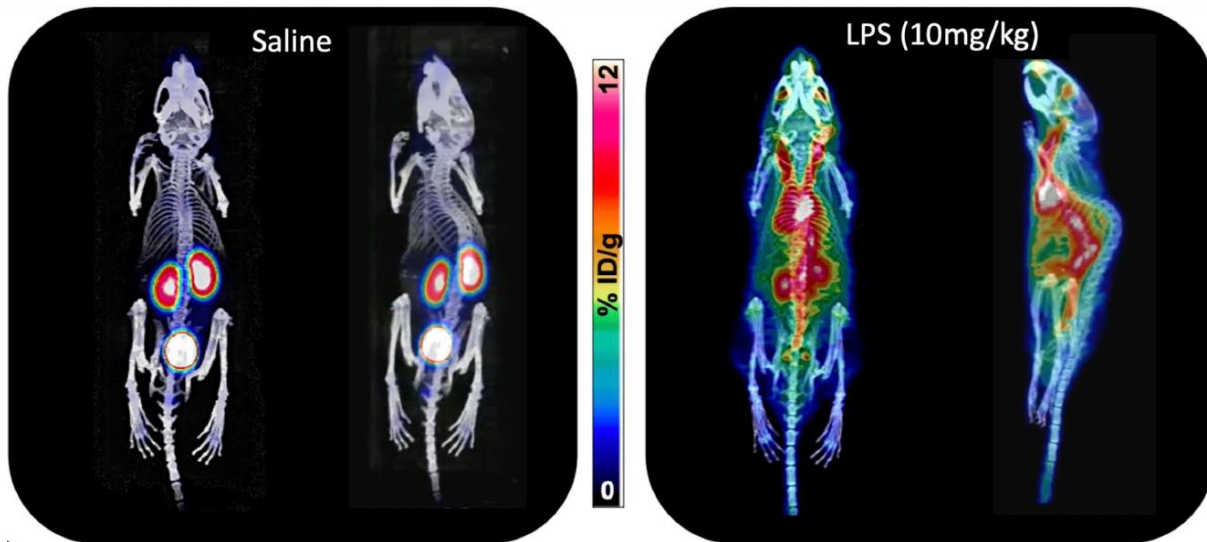


Figure 7. 50-60 minute summed whole-body PET/CT of control (left) and LPS (right) mice. Figure reproduced from Carlson WMIC 2021.

- 2) **Arthritis:** Macrophages are known to play a key role in arthritis.⁵⁰ In a female rat model of collagen-induced arthritis (CIA), where D4-Cy5 was administered 12 days after full model induction, D4-Cy5 selectively localized to activated macrophages in inflamed soft tissues of arthritic hindlimb joints (see **Figure 8**).⁵¹

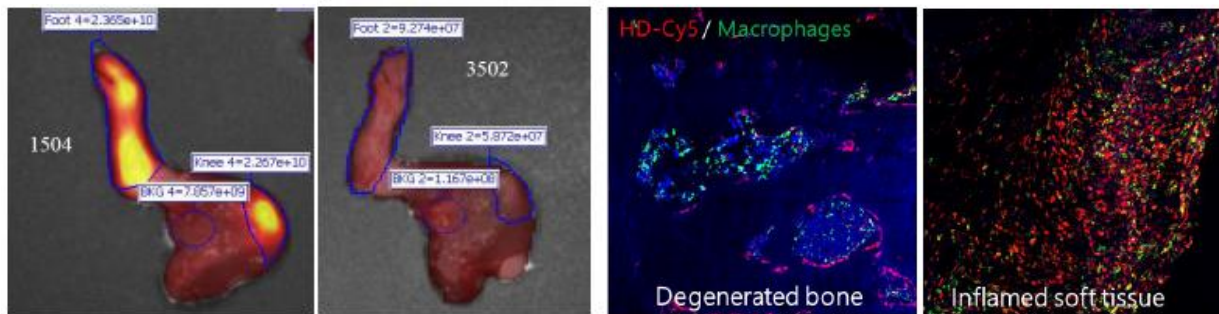


Figure 8. Selective localization of D4-Cy5 to activated macrophages in inflamed joints of rats in the CIA model. Figure reproduced from Cleland *et al.*, 2020.⁵¹

- 3) **Acute renal injury:** D4-Cy5 localized to renal macrophages <1-hour following reperfusion in an ischemia-induced acute kidney injury (AKI) model in streptozotocin-induced diabetic rats (see **Figure 9**).⁵²

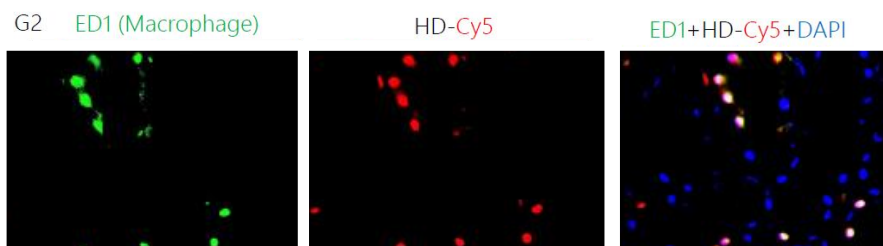


Figure 9. Renal macrophage localization of D4-Cy5 in a rat acute diabetic ischemia/reperfusion kidney injury model. Figure reproduced from Cleland *et al.*⁵²

- 4) **Acute myocardial infarction:** G6-Cy5 selectively localized to infiltrating macrophages in ischemic myocardium in a 30-minute temporary left anterior descending artery occlusion myocardial infarction rabbit model.⁵³ Furthermore, G4-NAC administration 30 minutes following resuscitation significantly improved survival, behavioral and motor outcomes in a cardiac arrest rat model.
- 5) **Acute lung injury:** G4-FITC was administered in the perfusate of an ex vivo rabbit model of acute lung injury where heart-lung blocks were harvested and exposed to 18 hours of cold ischemia and then reperfused.⁵⁴ G4-FITC showed a dose-response dependent accumulation in the lung, with ischemia/reperfusion lungs showing more G4-FITC labeling than control lungs. G4-FITC localized to pneumocytes in the alveoli and bronchioles as well as alveolar macrophages two hours after reperfusion.
- 6) **Neuromuscular disease:** G4 HD conjugated to 2-(phosphonomethyl) pentanedioic acid (G4-2PMPA), a GCP II inhibitor, was used to treat mice with the SOD1^{G93A} mutation, a model of amyotrophic lateral sclerosis (ALS).⁴⁶ G4-2PMPA could be administered at 5x lower doses and 3.5x less frequently than had been previously reported with free 2PMPA (twice weekly 20 mg/kg vs. daily 100 mg/kg). D-2PMPA-Cy5 specifically targeted macrophages in the gastrocnemius muscles of affected mice, and D-2PMPA treatment slowed both progression of limb weakness and neuromuscular junction (NMJ) denervation in SOD1^{G93A} mice, presumably secondary to GCP II inhibition in macrophages.⁵⁵

VI. HDs in the Clinic

1) HDs in the clinic in ocular and neurological diseases (Table 7)

[i\) D-4517.2 \(migladendranib\)](#)

MOA of D-4517.2

Activated microglia/macrophages and hypertrophic retinal pigment epithelium (hRPE) play an important role in wet AMD and the progression of CNV that is largely not addressed by current anti-VEGF therapies.⁵⁶⁻⁶⁰ Targeting and delivering anti-angiogenic drugs to these cells with HD nanomedicines has the potential to effectively suppress CNV formation and slow AMD progression.

Cell-based assays in human RPE cells (ARPE-19) demonstrate the anti-angiogenic MOA of D-4517.2.⁶¹ D-4517.2 reduces the expression of all VEGF isoforms (VEGF165, VEGF-A, and VEGF-C) in RPE cells exposed to hypoxic conditions. A similar reduction in VEGF expression was observed upon treatment of activated macrophages.⁶¹ Taken together, these results demonstrate that D-4517.2 inhibits angiogenesis through inhibition of VEGF expression and signaling (autocrine pathway). In addition, four studies in the laser-induced CNV mouse model and one study in the oxygen-induced retinopathy model showed consistent reduction of neovascularization after SC or oral dosing of D-4517.2 with efficacy equivalent or significantly better than IVT aflibercept control.^{34,62} D-4517.2 SC or oral dosing was efficacious in a spontaneous retinal neovascularization vldlr mouse model.⁶³

Completed and ongoing clinical studies with D-4517.2

Phase 1 human studies in healthy volunteers (N = 16) demonstrated that SC D-4517.2 was safe and well-tolerated at doses from 0.25 to 2 mg/kg. Human doses of 0.5 to 2 mg/kg are projected to yield exposure of ~1.8 to 14 h- μ g/mL, comparable to observed exposure of 1.2 to 4.7 h- μ g/ml that yielded efficacy in the laser-induced CNV mouse model.⁶¹ D-4517.2 did not have off-target toxicity (e.g., no liver toxicity) in chronic GLP toxicology studies (dogs/rats) or in the completed Phase 1 human clinical trial. D-4517.2 is in a Phase 2 clinical trial in patients with wet AMD or DME (see **Table 7**).

D-4517.2 has the potential to change the current treatment paradigm for wet AMD and DME by offering a systemic route of administration rather than delivery via IVT injection.

ii) OP-801 (“flurimedrimer”)

MOA of OP-801

The selective targeting of activated microglia/macrophages by the core G4 HD in OP-801 was demonstrated using a fluorescent version of OP-801 in multiple animal models of neurological diseases.^{13,16,38,42,45,48,54,64–66} Because G4 HDs are internalized only by activated microglia, OP-801 has a superior signal-to-noise profile compared to PET imaging agents such as 18 kDa TSPO that require ligand binding and do not discriminate between activated and resting cells. In the 5xFAD AD mouse model, OP-801 detected early-stage neuroinflammation with ~4-fold higher sensitivity than TSPO PET tracer.^{49,65} A fluorescent version of OP-801 accumulated in activated microglia associated with plaques, suggesting that OP-801 could image plaque-associated microglia in patients with Alzheimer’s disease.¹³ Importantly, OP-801 PET signal correlated with disease severity in animal models of inflammation, which may provide information on the stage and progression of neuroinflammatory diseases.^{47,64,67} Moreover, preclinical studies in an EAE mouse model of MS have shown that IV administered OP-801 sensitively detected spinal cord inflammation during the pre-symptomatic and symptomatic phases.⁴⁷

Ongoing clinical studies with OP-801

OP-801 is currently being evaluated in a Phase 1 clinical trial in healthy volunteers and patients with ALS. The aim of the trial is to study safety, pharmacokinetic and imaging parameters that will ultimately support its use as a biomarker of disease stage, progression and therapeutic efficacy.

iii) OP-101 (“acetylcysteine zidrimer”)

MOA of OP-101

OP-101 is selectively internalized by activated microglia and macrophages via fluid phase endocytosis. Following internalization, the intracellular reducing environment cleaves the disulfide bond, releasing NAC from OP-101. NAC restores glutathione levels and exerts anti-inflammatory actions through inhibition of the nuclear factor kappa beta (NF κ B) receptor, leading to reduction in pro-inflammatory cytokine expression.⁶⁸

In a rabbit model of CP, improvement of motor function in newborn kits was observed after a single 10 mg/kg IV dose of OP-101.¹⁰ Similarly, improvement of neurobehavioral function in a mouse model of

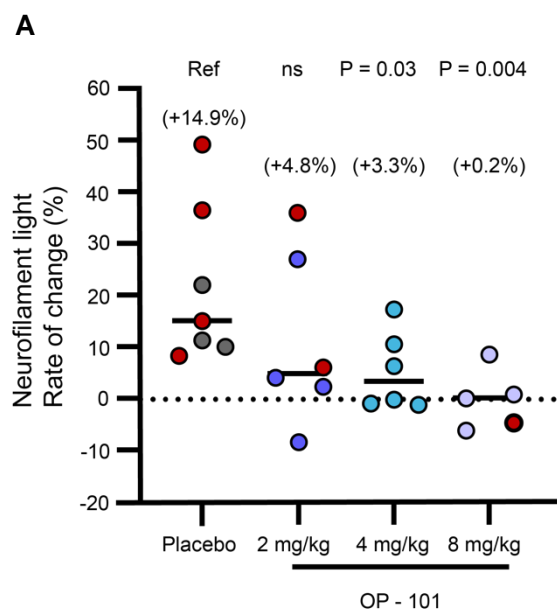
Rett syndrome was seen after administering 60 mg/kg of OP-101 twice per week.¹⁶ These doses correspond to ~4 to 8 mg/kg human equivalent doses (HEDs).

Completed trials with OP-101

OP-101 has been evaluated in two Phase 1 clinical trials in healthy volunteers and a Phase 2a study in patients with severe COVID-19 that demonstrated a significant reduction of inflammatory biomarkers and reduced inflammation. In the trial investigating OP-101 in healthy volunteers, near complete mass balance of OP-101 was detected in the urine after a single IV dose, indicating that the majority was directly excreted into the urine and therefore eliminated via a preferential renal clearance mechanism (unpublished). In the latter study, OP-101 demonstrated an excellent safety and tolerability profile. All treatment-emergent adverse events were determined to be caused by SARS-CoV-2 and the occurrence of adverse events was not different between patients treated with OP-101 or sham. OP-101 was rapidly cleared from the body with complete elimination from the plasma around 24 hours. Markers of kidney injury were also assessed and there was no difference between patient groups.

In addition to safety and tolerability, efficacy measures of inflammation and neuronal/astroglial damage attenuation were also reported. C-reactive protein, a molecule that increases in the plasma as inflammation increases within the body, decreased more in patients treated with OP-101 than those treated with sham. OP-101 attenuated the increase of several other inflammatory markers as well as markers of neuronal and astroglial damage as compared to placebo. Clinical outcomes following OP-101 treatment were favorable: survival was 67% to 100% for patients treated with OP-101, with patients receiving higher doses more likely to survive and only a 43% survival rate for those treated with placebo. Risk of mechanical ventilation or death at 30 days following treatment was 71% for placebo and 18% for treatment arms. Treatment with OP-101 also showed a tendency to induce more rapid improvement in disease severity (see **Table 7**).⁶⁹

Rate of change in neurofilament light chain (nFL) as a marker for neuroinflammation in patients with severe COVID-19



Time to hospital discharge or death in patients with severe COVID-19

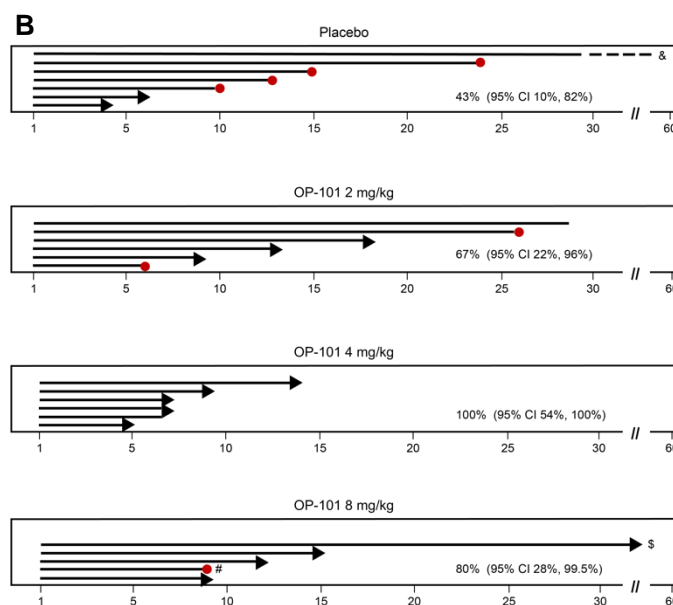


Figure 10. Clinical outcomes measured in severe COVID-19 patients treated with placebo or various dosages of OP-101. A) Datapoints representing patients who died are shown in red. Black horizontal bar represents the median change in treatment group patients with the corresponding value at the top under statistical significance for that group. Statistical significance was demonstrated in treatment group vs. placebo, but not amongst the three treatment group dosages. B) Patients who died are represented with a red circle. Patients who were discharged from the hospital are indicated with an arrowhead. Patients with novel circumstances are represented as follows: &) Patient required mechanical ventilation until the end of the study, \$) Patient had pre-existing hepatitis C virus infection and chronic liver failure and #) Patient was moved to palliative care per family request. Adapted from Gusdon *et al.*, 2022.⁶⁹

VII. Conclusion

Therapeutics have often suffered from a lack of precise targeting, resulting in reduced efficacy and increased off-target effects. Additionally, selective biological barriers hinder the treatment of disease beyond the BBB and/or require administration that causes significant patient burden, like IVT injections to bypass the BRB in the eye. Ashvattha is developing precision nanomedicine therapeutics that show remarkable specificity for regions of inflammation and disease. Healthy tissue remains untouched, and the therapy is excreted via the kidneys within 24-48 hours, demonstrating a favorable and dependable safety profile. By treating the disease at the source, Ashvattha's novel approach to precision medicine may minimize off-target effects after systemic administration and avoid creation of harmful metabolites by bypassing liver metabolism. This new class of precision nanomedicines has the potential to revolutionize the standard of care in ophthalmology, neurology, and inflammation with a preferential targeting of cells within regions of inflammation allowing a safe therapeutic option to address difficult-to-treat diseases.

VIII. Tables

Table 1. Dendrimer Characteristics

Property	HD	Flurimedrimer ([¹⁸ F]OP-801)	Migladendranib (D4517.2)	Acetylcysteine zidimer (OP-101)
Core	G4-PAMAM HD	G4-PAMAM HD with 10 alkynes	G4-PAMAM HD with 7 alkynes	G4-PAMAM HD with 22 amines
Dendrimer Molecule Weight	~14,000 Da	~16,000 Da	~19,000 Da	~21,000 Da
Chemical Formula	C ₆₂₂ H ₁₁₈₄ N ₁₈₆ O ₁₈₈	C ₇₀₂ H ₁₃₀₄ F ₁₀ N ₂₁₆ O ₁₉₈	C ₈₅₃ H ₁₄₆₄ F ₇ N ₂₃₅ O ₂₃₇	C ₈₈₆ H ₁₅₈₀ N ₂₃₀ O ₂₉₈ S ₄₄
Remaining Surface Hydroxyl Groups	64 (100%)	54 (84%)	57 (90%)	42 (66%)
Fraction of Mass Hydroxyl Dendrimer	100%	88%	75%	68%
Zeta potential	Neutral (+4.5 mV)	Nearly neutral (+5 mV)	Nearly neutral (+XX mV)	Nearly neutral (+ 6.5 mV)
Size (nm)	~4 nm	~4 nm	~4 nm	~4 nm
Small Molecule Linked to Dendrimer	-	18F	VEGF tyrosine kinase inhibitor	N-Acetyl-L-Cysteine 

Table 2. Ocular Localization

Model	Dendrimer	Age	Time After Injection to Analysis	Localized to Injury	Activated Cell Uptake	Ref.
Human eye cups from AMD patients	G4-Cy5	71-84y	6h	Sattler's layer of choroidal tissues in human eyecups	Macrophages	Kambhampati et al., 2021
Rat model of macular degeneration (subretinal lipid injection)	G4-TA-Cy5	6-7w	10d	Bleb area of choroidal tissues	RPE, macrophages, microglia	Kambhampati et al., 2021
Mouse model of retinopathy (oxygen induced)	G4-TA-Cy5	Injury: PND7-12, HD: PND15	2d	Inner retina vasculature	Microglia, macrophages	Cho et al., 2021
Royal College of Surgeons' rat model of retinal degeneration	G4-Cy5.5, G4-FITC	5w	24h, 72h, 10d	Inner retina and outer nuclear layer of the retina	Microglia	Iezzi et al., 2012
Mouse model of ischemia/reperfusion retinal injury	G4-Cy5	HD: 6d post injury	24h, 72h, 21d	<ul style="list-style-type: none"> Subretinal space, outer nuclear layer and inner nuclear layer Inner retina, subretinal space and RPE 	Microglia, macrophages, RPE	Kambhampati et al., 2015

Table 3. Ocular Efficacy

Conjugated Drug	Parent Molecule	G4/G6	Pro-drug	Model	Route	Dose	Efficacy	Ref.
D-TA	TA	G4	Y	Rat model of macular degeneration (subretinal lipid injection)	IV	3 or 10 mg/kg	<ul style="list-style-type: none"> D-TA significantly reduced choroidal neovascular formation by >80%, which is >50-fold better than TA D-TA suppressed several pro-inflammatory cytokines and pro-angiogenic factor expression under induced inflammation while TA suppressed far fewer D-TA reduced macrophage accumulation in the bleb area while TA did not 	Kambham pati et al., 2021
D-TA	TA	G4	Y	Mouse model of retinopathy (oxygen induced retinopathy)	IVT	0.1, 0.2, 0.5mg	<ul style="list-style-type: none"> D-TA suppressed retinal inflammatory cytokines, microglial activation, and pathological neovascularization better than TA D-TA protected neuro-retinal and visual function better than TA 	Cho et al., 2021
D-FA	FA	G4	Y	Royal College of Surgeons' rat model of retinal degeneration	IVT	1, 3 mg	<ul style="list-style-type: none"> D-FA improved the retinas ability to detect light more than FA D-FA treatment resulted in greater outer nuclear layer thickness than FA treatment 	Iezzi et al., 2012
D-4517.2	VEGFR tyrosine kinase	G4	N	Laser induced mouse model of neo-vascularization	D4517.2: SC or oral Aflibercept: IVT	D4517.2 SC: 40, 200 or 1000 ug or 10, 40 ug D4517.2 oral: 1000 or 5000 ug Aflibercept: 40 ug	<ul style="list-style-type: none"> A single SC dose of D-4517 (10 or 40 ug) resulted in comparable or better inhibition of CNV compared to single IVT injection of aflibercept (40 ug) Oral dose of D-4517 resulted in significantly better inhibition of CNV compared to single IVT injection of aflibercept (40 ug) Repeat dosages or single high dose of D-4517.2 did not result in any observed adverse effects Comparable doses of sunitinib demonstrated significant toxicity and mortality 	Cleland et al., 2021
D-4517.2	VEGFR tyrosine kinase inhibitor	G4	N	Laser induced rupture of Bruch's membrane in C57BL/6 mice	D4517.2: SC or oral Aflibercept: IVT	D4517.2 SC: 40 or 10, 40 ug D4517.2 oral: 40 or 200 ug Aflibercept: 40 ug	<ul style="list-style-type: none"> The CNV lesion area was significantly reduced in mice treated with SC D-4517.2 at 40 ug compared to vehicle control Oral dose of D-4517.2 provided superior efficacy with salcaprozate sodium (SNAC) excipient 	Le Moan et al., 2023

Table 4. CNS Localization

Model	Dendrimer	Age	Time After Injection to Analysis	Localized to Injury	Activated Cell Uptake	Biodistribution	Ref.
Rabbit model of CP (uterine injection with <i>E.coli</i> endotoxin)	G4-FITC, G4-Cy5, G4-NH ₂ -FITC	PND1	0.5, 4, 25h	Periventricular region Absent from cortex, corpus callosum, and subventricular zone	Microglia	Minimal accumulation in major organs except kidney, indicating renal clearance	Nance et al., 2016
Rabbit model of CP (uterine injection with <i>E.coli</i> endotoxin)	G4-Cy5	PND1	24h	Periventricular region	N/A	Minimal accumulation in major organs except kidney, indicating renal clearance	Lesniak et al., 2013
Rabbit model of CP (uterine injection with <i>E.coli</i> endotoxin)	G6-Cy5	PND1	PND4, PND15	Cortex and cerebellum	Microglia	N/A	Zhang et al., 2020
Rabbit Model of CP (uterine injection with <i>E.coli</i> endotoxin)	G4-FITC	PND1	24h	Periventricular brain region	Microglia, astrocytes	N/A	Kannan et al., 2012
Mouse model of CP	G4-NAC-Cy5	PND7 (injury)	0, 6, 24h	CA1 region of hippocampus Absent from CA3 region of hippocampus	Microglia	N/A	Nemeth et al., 2017
Mouse model of Alzheimer's disease (5xFAD)	G4-Cy5 G6-Cy5	7mo	48h	Plaque-associated microglia in hippocampus Absent from oligodendrocytes, astrocytes, and neurons	Microglia	N/A	Henningfield et al., 2020
Mouse model of Alzheimer's disease (C57BL/6J mice with AAV-hTau injection)	G4-Cy5 D-DPTIP	10w	6w	DG	Microglia	N/A	Tallon et al., 2022a
Mouse model of MS (EAE immunized)	G4-Cy5	10-12w (14d post-immunization)	24h	Molecular layer of DG Negligible uptake by astrocyte	Microglia	N/A	Hollinger et al., 2022
Mouse model of MS (EAE immunized)	[18F]OP-801-G4	12 w	60 min	Lumbar spinal cord Reduced uptake in treated and healthy mice	Microglia, macrophages	No significant difference in uptake by peripheral tissues	Carlson et al., 2022
Mouse model of Rett syndrome (Mecp2-null mice)	G4-Cy5	1w, 7w	24h	Corpus callosum Absent from astrocytes in brain slices and primary culture	Microglia	N/A	Nance et al., 2017

Canine model of hypothermic cardiac arrest resulting in brain injury	G6-Cy5	6-12m	10% before procedure 70% over 6h following procedure 20% 24h after procedure	Dentate gyrus and necrotic pyramidal neurons in hippocampus Absent from healthy neurons and astrocytes	Microglia	Minimal accumulation in the heart, lung, and pancreas Renal clearance was reduced and hepatic clearance was increased 4-fold with G6 HDs as compared to G4 HDs	Zhang et al., 2017
Rat model of cardiac arrest resulting in brain Injury	G4-Cy5	8-12 w	0.5h	Primary motor cortex, CA1 regions of the hippocampus and striatum	Microglia	N/A	Modi et al., 2022
Mouse model of necrotizing enterocolitis (NEC) resulting in brain inflammation	G4-Cy5	P10	PND11	Periventricular brain region and hippocampus	Microglia	N/A	Niño et al., 2018
Canine model of hypothermic cardiac arrest resulting in brain injury	G4-Cy5, G4-D-FITC	6-12m	24h after G4-Cy5	Dentate granule cell layer of the outer hippocampus, including injured neurons and Purkinje cells in the cerebellum	Microglia	Intra-cisterna magna and IV administration resulted in rapid renal clearance with low presence in other major organs	Mishra et al., 2014

Table 5. Efficacy in Animal Models of CNS Diseases

Conjugated Drug	Parent Molecule	G4/G6	Pro-drug	Model	Route	Dose	Efficacy	Ref.
D-NAC	NAC	G6	Y	Rabbit model of CP (uterine injection of E.coli endotoxin)	IV	2, 5 mg/kg	<ul style="list-style-type: none"> D-NAC decreased nitrite levels significantly better than NAC D-NAC significantly reduced microglia mediated inflammation in the cortex and cerebellum while NAC did not D-NAC improved survival rate and motor function of kits to levels similar to healthy controls 	Zhang et al., 2020
D-NAC	NAC	G4	Y	Rabbit model of CP (uterine injection of E.coli endotoxin)	IV	1, 10 or 60 mg/kg	<ul style="list-style-type: none"> D-NAC improved motor function and muscle tone significantly better than both an equivalent and a 10-fold higher dose of NAC D-NAC reduced inflammation and oxidative injury more than NAC D-NAC reduced proinflammatory microglia D-NAC improved microglial morphology to almost healthy cells while NAC was not as effective D-NAC significantly increased neuron number compared to NAC 	Kannan et al., 2012
D-NAC	NAC	G4	Y	Mouse model of CP	Injection	10 mg/kg	<ul style="list-style-type: none"> D-NAC microglial uptake correlated with severity of injury 	Nemeth et al., 2017

D-NAC, D-VPA	NAC, VPA	G4	Y	Canine model of hypothermic circulatory arrest	IV	10 mg/kg	<ul style="list-style-type: none"> D-NAC in combination with D-VPA produced improvements in neurological outcomes at 1/10th of the dose of NAC+VPA or VPA in addition to reduced side effects 	Mishra et al., 2014
D-NAC	NAC	G4	Y	Rat model of cardiac arrest resulting in brain injury	IV	60 mg/kg	<ul style="list-style-type: none"> D-NAC improved neurologic deficit scores and survival rate compared to saline treatment 	Modi et al., 2022
D-NAC	NAC	G4	Y	Mouse model of NEC	Oral	100 mg/kg	<ul style="list-style-type: none"> D-NAC reduced oxidant accumulation and microglial activation D-NAC prevented antioxidant depletion, demyelination, and neurocognitive impairments 	Niño et al., 2018
D-NAC	NAC	G4	Y	Mouse model of Rett Syndrome Mecp2-null)	IV	60 mg/kg OP-101	<ul style="list-style-type: none"> D-NAC decreased nitric oxide production at high and low concentrations, but NAC only decreased nitric oxide at the highest concentration in glial cells exposed to LPS D-NAC more efficiently attenuated the cytokine response than NAC in glial cells following LPS exposure D-NAC slowed progression compared to PBS control, but survival was not significantly improved NAC did not improve progression or survival 	Nance et al., 2017
D-DPTIP	DPTIP	G4	Y	Mouse model of Alzheimer's disease (C57BL/6J mice with AAV-hTau injection)	Oral	100 mg/kg	<ul style="list-style-type: none"> D-DPTIP pre-treatment prevented extracellular vesical release into plasma while DPTIP did not D-DPTIP reduced nSMase2 activity in the hippocampus but not the frontal cortex, as intended, no DPTIP data available D-DPTIP pre-treatment prevented the spread of tau 	Tallon et al., 2022a
D-2-PMPA	2-PMPA	G4	Y	Mouse model of MS (EAE-immunized)	IP	20 mg/kg	<ul style="list-style-type: none"> D-2-PMPA selectively targeted activated microglia in the brain and induced a >75% reduction in GCPII activity levels, leading to improved cognition compared to vehicle control 	Hollinger et al., 2022
D-2-PMPA	2-PMPA	G4	Y	Mouse model of ALS-peripheral nerves (SOD1 ^{G93A} mice)	IP	20 mg/kg	<ul style="list-style-type: none"> D-2-PMPA normalized enhanced GCPII activity, slowed the progression of limb weakness, and inhibited loss of NMJ compared to vehicle treated controls No improvements in weight, motor neuron protection, or survival in D-2-PMPA group 	Tallon et al., 2022b
DJHU29	JHU29	G4	Y	Mouse model of Rett Syndrome (Mecp2-null)	IP	60-100 mg/kg	<ul style="list-style-type: none"> D-JHU29 did not alter efficacy compared to JHU29 ex-vivo D-JHU29 inhibited microglia GLS activity in vivo compared to saline control D-JHU29 modestly improved movement velocity compared to saline-treated controls DJHU29 results did not differ from vehicle control for neurobehavioral 	Khoury et al., 2020

							score, paw clench score, respiratory function and learning	
D-cMK801	(cMK801)	G4	Y	Canine model of hypothermic circulatory arrest	IV	Low dose: 0.05 mg/kg Medium dose: 0.15 mg/kg High dose: 1.56 mg/kg	<ul style="list-style-type: none"> D-cMK801 improved neurobehavioral and histopathology scores 	Giuliano et al., 2020

DPTIP: 2,6-Dimethoxy-4-(5-Phenyl-4-Thiophen-2-yl-1H-Imidazol-2-yl)-Phenol; 2-PMPA: 2-(phosphonomethyl) pentanedioic acid;

cMK801: 10,11-Dihydro-5-methyl-5H-dibenzo[a,d]cyclohepten-5,10-imine-12-carboxylic acid (4,5-dimethoxy-2-nitrophenyl)methyl ester, Dizocilpine N-(4,5-dimethoxy-2-nitrobenzyl) carbamate

Table 6. Localization in Other Systemic Disease Models

Model	Dendrimer	Age	Time After Injection to Analysis	Localized to Injury	Activated Cell Uptake	Bio-distribution	Ref.
Rabbit model of ischemic reperfusion-injury in cardiac tissue	G6-Cy5	~5 mos	3,24,48h	Anterior myocardial wall	Macrophages	Minimal accumulation in major organs except for the kidney, indicating renal clearance	Magruder et al., 2017
Mouse model of ALS (SOD1 ^{G39A} mice)	G4-Cy5	12w	14w or until death	Gastrocnemius muscle	Macrophages	N/A	Tallon et al., 2022b
Rat model of AKI (induced diabetes with IP 70 mg/kg Streptozotocin)	G4-Cy5	4d	6, 24h post-surgery	Kidney	Renal macrophages	N/A	Cleland et al., 2020
Mouse model of sepsis (IP injection 10 mg/kg LPS)	[¹⁸ F]FOP-801	8-12 w	150m, 24h	Systemic (body and brain)	Activated microglia and macrophages	N/A	Carlson et al., 2021

Table 7. Clinical Trial Efficacy

Conjugated drug	Parent Molecule	Pro-dug	G4/G6	Model	Route	Dose	Efficacy	Ref.
OP-101	NAC	Y	G4	SAR-CoV-2 patients	IV	2, 4, 8 mg/kg	OP-101 risk of mechanical ventilation or death at 30 and 60d following treatment was 71% for placebo and 18% for treatment arms	Gusdon et al., 2022
D-4517.2	VEGF tyrosine kinase inhibitor	N	G4	Healthy volunteers	SC	0.25, 0.5, 1, 2 mg/kg	D4517.2 was well tolerated in doses translated from efficacious doses in the CNV mouse model	Cleland et al., 2022

IX. Literature Cited

1. Buhleier, E., Wehner, W. & Vogtle, F. 'Cascade' and 'Nonskid-Chain-like' Syntheses of Molecular Cavity Topologies. *Synthesis (Stuttg)* **3**, 155–158 (1978).
2. Tomalia, D. A. *et al.* A New Class of Polymers: Starburst-Dendritic Macromolecules. *Polymer Journal* vol. 17 (1985).
3. Balogh, L. P. Dendrimers 101. in *Advances in Experimental Medicine and Biology* vol. 620 (Landes Bioscience and Springer Science + Business Media LLC, 2007).
4. Carvalho, M. R., Reis, R. L. & Oliveira, J. M. Dendrimer nanoparticles for colorectal cancer applications. *J Mater Chem B* **8**, 1128–1138 (2020).
5. Sharma, A. *et al.* Dense hydroxyl polyethylene glycol dendrimer targets activated glia in multiple CNS disorders. *Sci Adv* **6**, 1–14 (2020).
6. Kambhampati, S. P. *et al.* Systemic and intravitreal delivery of dendrimers to activated microglia/macrophage in ischemia/reperfusion mouse retina. *Invest Ophthalmol Vis Sci* **56**, 4413–4424 (2015).
7. Kambhampati, S. P. *et al.* Systemic dendrimer nanotherapies for targeted suppression of choroidal inflammation and neovascularization in age-related macular degeneration. *Journal of Controlled Release* **335**, 527–540 (2021).
8. Cho, H. *et al.* Dendrimer-Triamcinolone Acetonide Reduces Neuroinflammation, Pathological Angiogenesis, and Neuroretinal Dysfunction in Ischemic Retinopathy. *Adv Ther (Weinh)* **4**, (2021).
9. Nance, E. *et al.* Nanoscale effects in dendrimer-mediated targeting of neuroinflammation. *Biomaterials* **101**, 96–107 (2016).
10. Kannan, S. *et al.* Dendrimer-based postnatal therapy for neuroinflammation and cerebral palsy in a rabbit model. *Sci Transl Med* **4**, (2012).
11. Alnasser, Y. *et al.* Preferential and Increased Uptake of Hydroxyl-Terminated PAMAM Dendrimers by Activated Microglia in Rabbit Brain Mixed Glial Culture. *Molecules* **23**, (2018).
12. Liaw, K., Gök, O., DeRidder, L. B., Kannan, S. & Kannan, R. M. Quantitative assessment of surface functionality effects on microglial uptake and retention of PAMAM dendrimers. *Journal of Nanoparticle Research* **20**, (2018).
13. Henningfield, C. M., Cleland, J. L., Sharma, R. & Green, K. N. Selective targeting of Plaque Associated Microglia through systemic dendrimer administration in an Alzheimer's disease model. AAIC Preprint at https://avtx.com/wp-content/uploads/Ashvattha-AAIC-2020-Poster_Final.pdf (2020).
14. Zhang, F., Nance, E., Alnasser, Y., Kannan, R. & Kannan, S. Microglial migration and interactions with dendrimer nanoparticles are altered in the presence of neuroinflammation. *J Neuroinflammation* **13**, (2016).

15. Nemeth, C. L. *et al.* Uptake of dendrimer-drug by different cell types in the hippocampus after hypoxic–ischemic insult in neonatal mice: Effects of injury, microglial activation and hypothermia. *Nanomedicine* **13**, 2359–2369 (2017).
16. Nance, E. *et al.* Dendrimer-mediated delivery of N-acetyl cysteine to microglia in a mouse model of Rett syndrome. *J Neuroinflammation* **14**, (2017).
17. Itagaki, S., Akiyama, H., Saito, H. & Mcgeer, P. L. *Ultrastructural localization of complement membrane attack complex (MAC)-like immunoreactivity in brains of patients with Alzheimer's disease.* *Brain Research* vol. 645 (1994).
18. Perlmutter, L., Scott, S., Barron, E. & Chui, H. *MHC Class 11-Positive Microglia in Human Brain: Association With Alzheimer Lesions.* *Journal of Neuroscience Research* vol. 33549458 (1992).
19. Sheng, J. G., Mrak, R. E. & Griffin, S. T. Neuritic plaque evolution in Alzheimer's disease is accompanied by transition of activated microglia from primed to enlarged to phagocytic forms. *Acta Neuropathologia* **94**, 1–5 (1997).
20. Frautschy, S. A. *et al.* *Animal Model Microglial Response to Amyloid Plaques in APPsw Transgenic Mice.* *American Journal of Pathology* vol. 152 (1998).
21. Giri, J. *et al.* Interactions of poly(amidoamine) dendrimers with human serum albumin: Binding constants and mechanisms. *ACS Nano* **5**, 3456–3468 (2011).
22. Haraldsson, B., Nyström, J. & Deen, W. M. Properties of the glomerular barrier and mechanisms of proteinuria. *Physiological Reviews* vol. 88 451–487 Preprint at <https://doi.org/10.1152/physrev.00055.2006> (2008).
23. Lesniak, W. G. *et al.* Biodistribution of fluorescently labeled PAMAM dendrimers in neonatal rabbits: Effect of neuroinflammation. *Mol Pharm* **10**, 4560–4571 (2013).
24. Zhang, F. *et al.* Generation-6 hydroxyl PAMAM dendrimers improve CNS penetration from intravenous administration in a large animal brain injury model. *Journal of Controlled Release* **249**, 173–182 (2017).
25. Mishra, M. K. *et al.* Dendrimer Brain Uptake and Targeted Therapy for Brain Injury in a Large Animal Model of Hypothermic Circulatory Arrest. *ACS Nano* **8**, 2134–2147 (2014).
26. Liaw, K. *et al.* Dendrimer size effects on the selective brain tumor targeting in orthotopic tumor models upon systemic administration. *Bioeng Transl Med* **5**, (2020).
27. Zhang, F. *et al.* Uniform brain tumor distribution and tumor associated macrophage targeting of systemically administered dendrimers. *Biomaterials* **52**, 507–516 (2015).
28. Patel, V. *et al.* Dendrimers as novel drug-delivery system and its applications. in *Drug Delivery Systems* 333–392 (Elsevier, 2019). doi:10.1016/B978-0-12-814487-9.00008-9.
29. Iezzi, R. *et al.* Dendrimer-based targeted intravitreal therapy for sustained attenuation of neuroinflammation in retinal degeneration. *Biomaterials* **33**, 979–988 (2012).

30. Iezzi, R. *et al.* Dendrimer-based targeted intravitreal therapy for sustained attenuation of neuroinflammation in retinal degeneration. *Biomaterials* **33**, 979–988 (2012).
31. Guo, Y. *et al.* Dendrimers target the ischemic lesion in rodent and primate models of nonarteritic anterior ischemic optic neuropathy. *PLoS One* **11**, (2016).
32. Kambhampati, S. P. *et al.* Systemic dendrimer nanotherapies for targeted suppression of choroidal inflammation and neovascularization in age-related macular degeneration. *Journal of Controlled Release* **335**, 527–540 (2021).
33. Le Moan, N., Culp, D. W., Marjoram, L., Dwadasi, V. & Cleland, J. Oral Formulation of the Anti-Angiogenesis Drug D4517.2 to Treat Age-Related Macular Degeneration (wet AMD) and Diabetic Macular Edema (DME). *ARVO Preprint at* (2023).
34. Cleland, J. L. *et al.* Single Subcutaneous (or Oral) Dose of Anti-Angiogenesis Drug Safely Suppresses Choroidal Neovascularization Comparable to Intravitreal Aflibercept. *ARVO Preprint at* https://avtx.com/wp-content/uploads/Ashvattha-ARVO-2021-Poster_Final.pdf (2021).
35. Modi, H. R. *et al.* Systemic administration of dendrimer N-acetyl cysteine improves outcomes and survival following cardiac arrest. *Bioeng Transl Med* **7**, (2022).
36. Hollinger, K. R. *et al.* Dendrimer-2PMPA selectively blocks upregulated microglial GCPII activity and improves cognition in a mouse model of multiple sclerosis. *Nanotheranostics* **6**, 126–142 (2022).
37. Tallon, C. *et al.* Dendrimer-2PMPA Delays Muscle Function Loss and Denervation in a Murine Model of Amyotrophic Lateral Sclerosis. *Neurotherapeutics* **19**, 274–288 (2022).
38. Mishra, M. K. *et al.* Dendrimer Brain Uptake and Targeted Therapy for Brain Injury in a Large Animal Model of Hypothermic Circulatory Arrest. *ACS Nano* **8**, 2134–2147 (2014).
39. Henningfield, C. M., Cleland, J. L., Sharma, R. & Green, K. N. Selective targeting of Plaque Associated Microglia through systemic dendrimer administration in an Alzheimer’s disease model. *AAIC Preprint at* (2020).
40. Henningfield, C. Unpublished Manuscript. *Manuscript in preparation* (2023).
41. Khoury, E. S. *et al.* Dendrimer-conjugated glutaminase inhibitor selectively targets microglial glutaminase in a mouse model of Rett syndrome. *Theranostics* **10**, 5736–5748 (2020).
42. Tallon, C. *et al.* Dendrimer-Conjugated nSMase2 Inhibitor Reduces Tau Propagation in Mice. *Pharmaceutics* **14**, (2022).
43. Zhang, Z. *et al.* Systemic dendrimer-drug nanomedicines for long-term treatment of mild-moderate cerebral palsy in a rabbit model. *J Neuroinflammation* **17**, (2020).
44. Modi, H. R. *et al.* Systemic administration of dendrimer N-acetyl cysteine improves outcomes and survival following cardiac arrest. *Bioeng Transl Med* **7**, (2022).

45. Niño, D. F. *et al.* Cognitive impairments induced by necrotizing enterocolitis can be prevented by inhibiting microglial activation in mouse brain. *Sci. Transl. Med* vol. 10 <http://stm.sciencemag.org/> (2018).
46. Tallon, C. *et al.* Dendrimer-2PMPA Delays Muscle Function Loss and Denervation in a Murine Model of Amyotrophic Lateral Sclerosis. *Neurotherapeutics* **19**, 274–288 (2022).
47. Carlson, M. L. *et al.* Development and initial assessment of [18 F]OP-801: a novel hydroxyl dendrimer PET tracer for imaging maladaptive inflammation in the whole body and brain Radiochemistry. *Manuscript Submitted* (2023).
48. Hollinger, K. R. *et al.* Dendrimer-2PMPA selectively blocks upregulated microglial GCPII activity and improves cognition in a mouse model of multiple sclerosis. *Nanotheranostics* **6**, 126–142 (2022).
49. Carlson, M. Development of 18F-OP-801: a novel hydroxyl dendrimer PET tracer for imaging maladaptive inflammation in the whole body and brain. *WMIC Preprint* at https://avttx.com/wp-content/uploads/Ashvattha-WMIC-2021-Talk-on-18F-OP-801-in-LPS-Mice_Final.pdf (2021).
50. Wynn, T. A., Chawla, A. & Pollard, J. W. Macrophage biology in development, homeostasis and disease. *Nature* vol. 496 445–455 Preprint at <https://doi.org/10.1038/nature12034> (2013).
51. Cleland, J., Sharma, R., Sun, M., Appiani La Rosa, S. & Kannan, R. M. Systemic Administration of Novel Hydroxyl Dendrimers to Target Inflammation in Arthritic Tissues. *ACR Convergence Preprint* at (2020).
52. Cleland, J. L. *et al.* Systemic Therapies Targeted to Ischemia in a Model of Diabetic Acute Kidney Injury. *ASN Preprint* at https://avttx.com/wp-content/uploads/Ashvattha-ARVO-2020-Presentation-3974-Session-429_Final.pdf (2020).
53. Magruder, J. T. *et al.* Selective Localization of a Novel Dendrimer Nanoparticle in Myocardial Ischemia-Reperfusion Injury. in *Annals of Thoracic Surgery* vol. 104 891–898 (Elsevier USA, 2017).
54. Grimm, J. C. *et al.* Accumulation and cellular localization of nanoparticles in an ex vivo model of acute lung injury. *Journal of Surgical Research* **210**, 78–85 (2017).
55. Tallon, C. *et al.* Dendrimer-2PMPA Delays Muscle Function Loss and Denervation in a Murine Model of Amyotrophic Lateral Sclerosis. *Neurotherapeutics* **19**, 274–288 (2022).
56. Ambati, J., Atkinson, J. P. & Gelfand, B. D. Immunology of age-related macular degeneration. *Nature Reviews Immunology* vol. 13 438–451 Preprint at <https://doi.org/10.1038/nri3459> (2013).
57. Holz, F. G., Strauss, E. C., Schmitz-Valckenberg, S. & Van Lookeren Campagne, M. Geographic atrophy: Clinical features and potential therapeutic approaches. *Ophthalmology* vol. 121 1079–1091 Preprint at <https://doi.org/10.1016/j.ophta.2013.11.023> (2014).
58. Lad, E. M., Cousins, S. W., Van Arnam, J. S. & Proia, A. D. Abundance of infiltrating CD163+ cells in the retina of postmortem eyes with dry and neovascular age-related macular degeneration. *Graefe's Archive for Clinical and Experimental Ophthalmology* **253**, 1941–1945 (2015).

59. Bhutto, I. & Luty, G. Understanding age-related macular degeneration (AMD): Relationships between the photoreceptor/retinal pigment epithelium/Bruch's membrane/choriocapillaris complex. *Molecular Aspects of Medicine* vol. 33 295–317 Preprint at <https://doi.org/10.1016/j.mam.2012.04.005> (2012).
60. Fritsche, L. G. *et al.* A large genome-wide association study of age-related macular degeneration highlights contributions of rare and common variants. *Nat Genet* **48**, 134–143 (2016).
61. Cleland, J. L., Sharma, R., Appiani La Rosa, S., Moore, J. & Rogers, B. Safety and Tolerability of a Single Subcutaneous Dose of Anti-Angiogenesis Drug to Treat Age-related Macular Degeneration (Wet AMD) and Diabetic Retinal Edema (DME). *ARVO Annual Meeting* Preprint at (2022).
62. Le Moan, N., Culp, D., Marjoram, L., Dwadasi, V. & Cleland, J. Oral Formulation Development of the Anti-Angiogenesis Drug D-4517.2 to Treat Age-related Macular Degeneration (wet AMD) and Diabetic Macular Edema (DME). *ARVO* Preprint at (2023).
63. Wu, S. *et al.* Suppression of subretinal neovascularization in Vldlr knockout mice by systemic administration of a targeted VEGF-receptor inhibitor . *ARVO* Preprint at (2023).
64. Carlson, M. Specific detection of pathogenic myeloid cells in a mouse model of multiple sclerosis using [18 F]OP-801 before and after treatment with a CSF1R inhibitor. Preprint at <https://avttx.com/wp-content/uploads/Carlson-et-al-18F-OP-801-WMIC-2022.pdf> (2022).
65. Carlson, M. L. *et al.* Novel hydroxyl dendrimer PET tracer [18F]OP-801 detects early-stage neuroinflammation in 5XFAD mouse model with higher sensitivity than TSPO-PET. *AAIC* Preprint at https://avttx.com/wp-content/uploads/Ashvattha-AAIC-2022-Poster_Final.pdf (2022).
66. Modi, H. R. *et al.* Systemic administration of dendrimer N-acetyl cysteine improves outcomes and survival following cardiac arrest. *Bioeng Transl Med* **7**, (2022).
67. Jackson, I. M. *et al.* Clinical Radiosynthesis and Translation of [18 F]OP-801: A Novel Radiotracer for Imaging Reactive Microglia and Macrophages. *Manuscript Submitted* (2023).
68. Turk, B. R. *et al.* Dendrimer–N-acetyl-L-cysteine modulates monophagocytic response in adrenoleukodystrophy. *Ann Neurol* **84**, 452–462 (2018).
69. Gusdon, A. M. *et al.* Dendrimer nanotherapy for severe COVID-19 attenuates inflammation and neurological injury markers and improves outcomes in a phase2a clinical trial. *Sci. Transl. Med* vol. 14 <https://www.science.org> (2022).